Nucleic Acids Research, 2025, **53**, gkaf181
https://doi.org/10.1093/nar/gkaf181
Chemical Biology and Nucleic Acid Chemistry

Enhanced or reversible RNA N6-methyladenosine editing by red/far-red light induction

Heng Tang[1,†], Shaoqin Han[2,†], Yang Jie[3,4,†], Xin Jiang[2], Yi Zhang[1], Junran Peng[2], Fang Wang[5], Xiang Li[1], Xiang Zhou[2,6], Wei Jiang[3,*], Xiaocheng Weng[1,2,6,*]

[1]Department of Otorhinolaryngology-Head and Neck Surgery, Department of Neurosurgery, Zhongnan Hospital of Wuhan University, Wuhan University, Wuhan 430072, China
[2]College of Chemistry and Molecular Sciences, Key Laboratory of Biomedical Polymers of Ministry of Education, Hubei Province Key Laboratory of Allergy and Immunology, Wuhan University, Wuhan 430072, P.R. China
[3]Department of Biological Repositories, Frontier Science Center for Immunology and Metabolism, Medical Research Institute, Zhongnan Hospital of Wuhan University, Wuhan University, Wuhan 430071, China
[4]State Key Laboratory of Biocatalysis and Enzyme Engineering, School of Life Science, Hubei University, Wuhan 430062, China
[5]Wuhan University School of Pharmaceutical Sciences, Wuhan University, Wuhan 430071, China
[6]Taikang Center for Life and Medical Sciences, Wuhan University, Wuhan, Hubei 430072, P.R. China

[*]To whom correspondence should be addressed. Email: xcweng@whu.edu.cn
Correspondence may also be addressed to Wei Jiang. Email: jiangw.mri@whu.edu.cn
[†]These authors contributed equally to this work.

Abstract

The RNA N6-methyladenosine (m^6A) modification is a critical regulator of various biological processes, but precise and dynamic control of m^6A remains a challenge. In this work, we present a red/far-red light-inducible m^6A editing system that enables efficient and reversible modulation of m^6A levels with minimal off-target effects. By engineering the CRISPR dCas13 protein and sgRNA with two pairs of light-inducible heterodimerizing proteins, ΔphyA/FHY1 and Bphp1/PspR2, we achieved targeted recruitment of m^6A effectors. This system significantly enhances m^6A writing efficiency and allows dynamic regulation of m^6A deposition and removal on specific transcripts, such as *SOX2* and *ACTB*. Notably, reversible m^6A editing was achieved through cyclic modulation at a single target site, demonstrating the ability to influence mRNA expression and modulate the differentiation state of human embryonic stem cells. This optogenetic platform offers a precise, versatile tool for cyclic and reversible m^6A regulation, with broad implications for understanding RNA biology and its potential applications in research and medicine.

Graphical abstract

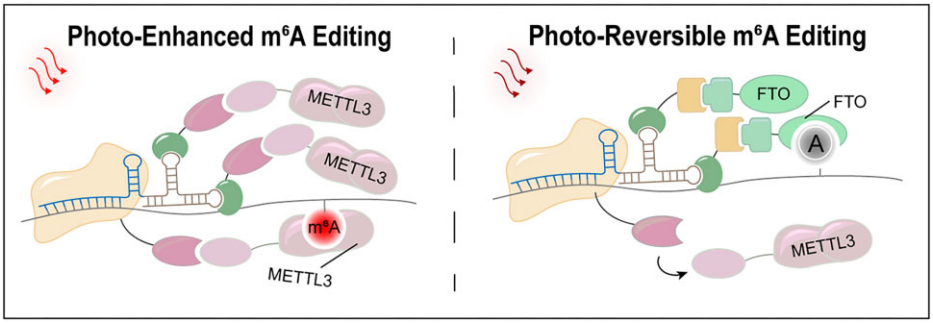

Introduction

Over the past few decades, >170 types of post-transcriptional RNA modifications have been identified, with N6-methyladenosine (m^6A) emerging as the most abundant and dynamic modification in eukaryotic mRNA (messenger RNA) [1, 2]. m^6A plays a critical role in regulating gene expression through a coordinated network of effectors, including methyltransferases ("writers" such as METTL3/METTL14/WTAP) [3–5], demethylases ("erasers" such as ALKBH5 and FTO (Fat Mass and Obesity-Associated)) [6, 7], and binding proteins ("readers" such as YTH domain and IGF2BP family proteins) [8, 9]. These components dynamically modulate m^6A [10] and influence processes such as mRNA stability [8], translation [11], termination [12], and splicing [13, 14], highlighting m^6A's essential functions in cellular biology [15–17].

Received: June 3, 2024. **Revised:** January 3, 2025. **Editorial Decision:** February 19, 2025. **Accepted:** February 25, 2025

Recent advances in CRISPR-based technologies [18–21] have enabled precise m^{6}A editing [22–25], providing valuable tools for dissecting the roles of m^{6}A in RNA regulation. While these technologies offer powerful tools for studying and adjusting RNA modifications with accuracy, there remains room for improvement in dynamic regulation. To address these challenges, innovative CRISPR-based m^{6}A editing systems employing chemical or photo-activatable controls have been developed for temporally precise m^{6}A manipulation [26–30]. However, limitations such as low editing efficiency, short excitation wavelengths of photo-irradiation and the lack of cyclic reversible switching highlight the necessity for further refinement.

The red/far-red light-inducible heterodimerizing proteins ΔphyA/FHY1 and Bphp1/PspR2 [31–34], when coupled with nucleic acid-specific binding proteins (such as dCas and TetR) and transcriptional activation promoters (e.g. VP16), enable optogenetic control over downstream gene activity with precise light stimulation [35, 36]. These systems demonstrate substantial potential for spatial and temporal modulation of RNA modifications within cellular environments [26, 37]. Notably, the deeper tissue penetration of red and far-red light wavelengths compared to shorter wavelengths enhances the viability of *in vivo* applications for light-inducible RNA editing [38, 39].

Here, we describe a photoregulated RNA m^{6}A editing system that enhances editing efficiency and enables reversible modulation. By engineering both dCas13 and sgRNA (single guide RNA) with the light-inducible heterodimerizing proteins ΔphyA/FHY1 and Bphp1/PspR2, the system achieves efficient recruitment of m^{6}A effectors to target sites. The reciprocal binding behavior of these proteins under red and far-red light allows precise, wavelength-dependent control. Specifically, m^{6}A writers and erasers are recruited or released in response to alternating light stimuli, enabling dynamic and reversible editing of RNA m^{6}A sites with high spatial and temporal resolution.

In this study, we demonstrate a significant increase in m^{6}A writing efficiency when both dCas13 and sgRNA are engineered to enhance METTL3 recruitment. Our system enables spatiotemporally controlled, reversible m^{6}A editing through simple switching between red and far-red light. Minimal off-target effects were observed, as confirmed by m^{6}A-seq and single-nucleotide quantification, underscoring its high specificity. Notably, by precisely modulating m^{6}A at specific mRNA sites, we show that dynamic regulation of m^{6}A not only alters mRNA levels but also influences stem cell differentiation. This work introduces a versatile optogenetic platform for precise RNA epigenetic regulation, providing a highly specific and minimally invasive method for controlling cellular functions.

Materials and methods

Plasmid construction

ΔphyA-nls-dCas13b-3 x FLAG: ΔphyA (1–617 aa) and dPspCas13b were polymerase chain reaction (PCR)-amplified from pYZ181 and phage-nls-dPspCas13b, respectively, and cloned into PB-CAG-BGHpA (Addgene, #92161) to construct ΔphyA-nls-dCas13b-3 x FLAG.

FHY1-M3 variants: M3 (METTL3 variants lacking zinc finger RNA-binding motifs), M3M14, and inactive M3 were PCR-amplified from pCMV-dCas13-M3nls (Addgene, #155366), pCMV-dCas13-M3M14nes (Addgene, #155367), and pCMV-dCas13-inactive M3 (Addgene, #157854). FHY1 was amplified from pDQ16 and both were cloned into PB-CAG-BGHpA to construct FHY1-M3-3 x FLAG, FHY1-M3M14-3 x FLAG, and FHY1-inactive M3-3 x FLAG. The FHY1-M3-3 x FLAG construct was further fused with PB-CAG-ΔphyA-dCas13b-3 x FLAG-BGHpA.

ΔphyA-MCP and PspR2-MCP variants: MS2 bacteriophage coat protein (MCP) was synthesized and fused with ΔphyA and PspR2 (amplified from pKA-142, Addgene, #79835), resulting in ΔphyA-MCP-3 x FLAG and PspR2-MCP-3 x FLAG.

Bphp1-FTO-3 x FLAG: FTO was PCR-amplified from psT1374-scFv-XTEN-FTO and fused with Bphp1 (amplified from pKA-141, Addgene, #79832). The fusion was cloned into PB-CAG-BGHpA along with PspR2-MCP-3 x FLAG to generate PB-CAG-PspR2-MCP-3 x FLAG-CMV-Bphp1-FTO-3 x FLAG-BGHpA.

Guide RNA constructs: To enhance effector recruitment, a 2 × MS2-binding module was appended to the 3′ end of sgRNA. Engineered sgRNA scaffolds were synthesized and cloned into pC0043 to create pC0043-U6-sgRNA-3′-2xMS2 (Supplementary Table S1). Guide RNAs were then annealed and cloned into this plasmid (Supplementary Table S2).

The PCR reactions were performed with DreamTaq 2x mix (Invitrogen) with the following program: preheat at 95°C for 3 min, 35 cycles of 3-step amplification (95°C for 30 s, 55–60°C for 30 s, and 72°C for 1 min), and final extension at 72°C for 5 min. PCR products were purified from agarose gel after separation by electrophoresis. The purified fragments and carriers ligated with T4 DNA ligase (Invitrogen). Ligation products were transformed into 50 μl of DH5α competent cells, and the bacteria were spread on LB plates with 100 μg·ml^{-1} ampicillin or 50 μg·ml^{-1} kanamycin. All plasmid sequences were verified by Sanger sequencing.

Mammalian cell culture and transfection

HEK293T and HeLa cells were maintained using Dulbecco's modified Eagle's medium (DMEM) (high glucose) supplemented with 10% fetal bovine serum (FBS), and 1% penicillin/streptomycin (Beijing Dingguo changsheng Biotechnology Co., Ltd, GA3502). Plasmid transfection was achieved using Lipofectamine 3000 (Invitrogen) following the manufacturer's protocol. For light-induced protein interaction assay, HEK293T/Hela cells plated on 35-mm glass bottom dish (Nest) were cotransfected with ΔphyA (1–617 aa)-dCas13-mcherry-CAAX/FHY1-M3-EGFP or PspR2-MCP-mVenus-CAAX/Bphp1-FTO-mCherry at mass ration of 1:1. For targeted m^{6}A editing, cells were cotransfected with effector, anchor, and sgRNA at a mass ration of 1:1:1.

Expression of proteins

HEK293T cells were plated in six-well plates. At 70%–80% confluency after plating, cells were transfected corresponding plasmid. After 24 h, cells were washed with phosphate-buffered saline (PBS) once and lysed with 200 μl of 1× SDS Loading buffer (10 mM Tris–HCl, pH 8.0, 50 mM DTT (Dithiothreitol), 1% SDS, 10% glycerol, and 0.008% bromophenol blue) at room temperature for 10 min and then denatured at 95°C for 10 min. The appropriate amount of protein was loaded onto SDS–PAGE gels. After separating proteins by running gel at a constant voltage of 100 V

for 1.5 h, proteins were transferred from gel onto a PVDF (Polyvinylidene Fluoride) membrane (Millipore) in an ice-bath for 2 h. Then, the PVDF membrane was blocked in 5% (w/v) BSA (Beijing Dingguo changsheng Biotechnology Co., Ltd, FA016) in TBST (Tris-buffered saline, 0.1% Tween 20) at room temperature for 1 h. The blot of protein was stained as indicate for at least 12 h at 4°C. The blot was washed four times with TBST at room temperature for 5 min each, and then stained with 1:5000 HRP-conjugated Affinipure Goat Anti-Rabbit IgG (H + L) (Proteintech, SA00001-2) or HRP-conjugated Affinipure Goat Anti-Mouse IgG (H + L) (Proteintech, SA00001-1) in 5% BSA (w/v) in TBST for 1 h at room temperature. The blots were washed four times with TBST at room temperature for 5 min each time and imaged on Molecular Imager ChemiDocTM XRS + Imaging System (Bio-Rad) after incubation with Rhea ECL (US Everbright, Inc).

FHY1-EGFP and Bphp1-FTO translocation assay

Cells cultured in confocal vessels and transfected with desired plasmids were imaged after 24 h transfection. Images were acquired with a microscope (DMIRB; Leica Biosystems) equipped with an EMC CD camera (iXon-897D; Andor Technology) and mounted with a ×2 magnification adapter and ×63 oil objective lens (NA 1.4). Basically, 488-nm and 638-nm excitation lasers were used for EGFP/mVenus, mCherry fluorescence excitations, respectively. Correspondingly, 498–542 nm and 650–700 nm emission signals were acquired. All fluorescence imaging data were analyzed by Fiji/ImageJ (https://imagej.net/Welcome).

RNA isolation

Cells were harvested and total RNA was extracted using TRIzol reagent (Invitrogen) following the manufacturer's protocol. To isolate mRNA and non-ribosomal (non-Rib) RNA from total RNA, the Oligo d (T)25 (NEB, S1419S) and rRNA Depletion Kit (Vazyme) were used separately according to the manufacturer's instructions. The RNA concentration was determined using a NanoDrop (Invitrogen) by measuring the UV absorbance at 260 nm

m^{6}A-IP and RT-qPCR

A total of 3×10^7 cells were lysed with Trizol. m^{6}A-IP was performed using the EpiMark N^6-Methyladenosine Enrichment Kit (NEB) according to the manufacturer's protocol. In brief, total RNA was isolated and then mRNA was further purified by Oligo d (T)25 beads twice. Poly (A)-enriched RNA was fragmented in solution of 50 mM Tris–HCl, pH 8.0, 50 mM $MgCl_2$, and heated at 95°C for exactly 8 min, and the mRNA fragments was purified with RNA Clean & Concentrator Kit (Zymo Research). A portion was saved as input RNA, remaining fragmented RNA was subjected to m^{6}A immunoprecipitation. 30 μl of protein G magnetic beads (NEB) were washed twice by IP reaction buffer (150 mM NaCl, 10 mM Tris–HCl, pH 7.5, and 0.1% NP-40 in nuclease-free H_2O), resuspended in 500 μl of reaction buffer, and tumbled with 5 μg of anti-m^{6}A antibody (NEB) at 4°C overnight. After two washes in reaction buffer, the antibody–bead mixture was resuspended in 500 μl of the reaction mixture containing fragmented RNA, 100 μl of reaction buffer, and 5 μl of RNasin Plus RNase Inhibitor, and incubated for at least 4 h at 4°C. To remove unbound RNA, samples were washed 5× with each of the following buffers: reaction buffer (150 mM NaCl, 10 mM Tris–HCl, pH 7.5, and 0.1% NP-40 in nuclease-free H_2O), low-salt reaction buffer (50 mM NaCl, 10 mM Tris–HCl, pH 7.5, and 0.1% NP-40 in nuclease-free H_2O), and high-salt reaction buffer (500 mM NaCl, 10 mM Tris–HCl, pH 7.5, and 0.1% NP-40 in nuclease-free H_2O). RNA was eluted in RLT buffer (Qiagen) and purified with RNA Clean & Concentrator kits. The purified RNA before or after m^{6}A IP was reverse transcribed into cDNA (complementary DNA), and qPCR (quantitative Polymerase Chain Reaction) assay was performed to analyze the m^{6}A enrichment. The qPCR was performed using Hieff qPCR SYBR Green Master Mix (Yeasen) in CFX96 Real-Time System (Bio-Rad, USA) (Supplementary Table S3).

SELECT

First 2 μg mRNA or non-Rib RNA was mixed with 40 nM Up Primer, 40 nM Down Primer and 5 μM dNTP in 17 μl of 1 × CutSmart buffer (50 mM KAc, 20 mM Tris-HAc, 10 mM MgAc2, 100 μg/ml BSA (Bovine Serum Albumin), pH 7.9 at 25°C) (Supplementary Table S4). The RNA and primers were annealed by incubating mixture at a temperature gradient: 90°C for 1 min, 80°C for 1 min, 70°C for 1 min, 60°C for 1 min, 50°C for 1 min, and then 40°C for 6 min. Subsequently, a 3 μl of mixture containing 0.01 U Bst 2.0 DNA polymerase, 0.5 U SplintR ligase, and 10 nmol ATP was added in the former mixture to the final volume 20 μl. The final reaction mixture was incubated at 40°C for 20 min, denatured at 80°C for 20 min, and kept at 4°C. Afterward, quantitative real-time PCR was performed on a CFX96 Real-Time System (Bio-Rad, USA). The 20 μl of qPCR reaction was composed of 2× Hieff qPCR SYBR Green Master Mix (Yeasen), 200 nM qPCRF primer, 200 nM qPCRR primer, 3 μl of the final reaction mixture, and ddH2O. qPCR was run at the following condition: 95°C, 5 min; (95°C, 10 s; 60°C, 20 s; 72°C, 20 s) × 40 cycles; 95°C, 15 s; 60°C, 1 min; 95°C, 15 s (collect fluorescence at a ramping rate of 0.05°C/s); 4°C, hold.

CLIP for FHY1-M3 enrichment

HEK293T cells was plated in 15-cm dishes and cotransfected with 10 μg ΔphyA (1–617 aa)-dPspCas13b-CMV-MCP-ΔphyA, 10 μg FHY1-M3, and 10 μg sgRNA. After 24 h post-transfection, some of them were illuminated with red light (10 s on, 50 s off) for 24 h later, cells were washed by ice-cold PBS once and then fixed by 1% paraformaldehyde at 37°C. for 10 min. After fixation, 125 mM glycine was added to quench cross-linking and incubated at room temperature for another 10 min. Cells were washed with ice-cold PBS twice and harvested by scraping, followed by centrifugation at 1000 × *g* for 5 min. The cell pellets were resuspended and lysed with 600 μl of RIPA Buffer (Solarbio) supplemented with RNase inhibitor (Thermo) and 1 mM PMSF (Phenylmethylsulfonyl Fluoride). Cells were incubated on ice for 30 min and sonicated for 5 min with a 30 s on/30 s off-cycle on a ultrasound instrument, followed by centrifugation at 16 000 × *g* for 10 min at 4°C. The clear supernatant containing lysate was then used for RNA–protein IP.

For RNA–protein IP, 35 μl of Dynabeads Protein G were washed with 200 μl of wash buffer (PBS with 0.02% Tween 20). Then, 5 μg of anti-METTL3 antibody was added and incubated on a rotator for 30 min at 4°C. After that, beads were carefully washed with wash buffer twice and resuspended in 250 μl of RIPA buffer supplemented with PMSF and RNase

inhibitor. In all, 250 μl of above lysate was added and rotated at 4°C overnight. After incubation, beads were washed with wash buffer twice and proteins were digested by Proteinase K (NEB) and incubated at 55°C for 2 h. RNA was purified with RNA Clean & Concentrator kits (Zymo Research). Purified RNA was reverse-transcribed and quantified with qPCR described above. The purified RNA before or after IP was reverse-transcribed into cDNA, and qPCR assay was performed to analyze the m^{6}A enrichment.

mRNA stability assay

HEK293T cells plated in 15-cm dishes, and transfected with 10 μg ΔphyA (1–617 aa)-dPspCas13b-CMV-MCP-ΔphyA, 10 μg FHY1-M3, and 10 μg sgRNA. After 24 h post-transfection, some of them were illuminated with red light (10 s on, 50 s off) for 24 h. Washing with PBS, total RNA was isolated by TRIzol and mRNA purified twice by oligo dT25. After reverse transcription, mRNA levels of target transcripts were analyzed by qPCR. GAPDH was used as the internal control for ACTB analysis, and ACTB was used as the internal control for GAPDH, FOXM1, and SOX2.

m^{6}A impact on mRNA translation

HEK293T cells seeded in 15-cm dishes were transfected with different components of the m^{6}A modification system and grown for 24 h, followed by illuminated with red light and grown for another 24 h before harvest. Proteins were extracted as mentioned above, and 20 μg of whole proteins was loaded for protein gel electrophoresis. GAPDH, FOXM1, SOX2, ACTB, and internal control proteins including Vinculin and GAPDH were probed with the corresponding anti-GAPDH antibody (ABclonal, #AC002, 1:10 000 dilution), anti-FOXM1 (Proteintech, #13147-1-AP, 1:5000 dilution), anti-SOX2 (Proteintech, #11064-1-AP, 1:1000 dilution), anti-β-actin (High Dilution) (ABclonal, -#AC026, 1:50 000 dilution), anti-Vinculin (proteintech, #66305-1-Ig, 1:5000 dilution), and corresponding secondary antibodies as described above.

m^{6}A dot blot

RNA was isolated from transfected cells. Equal amounts of RNA were dropped on a nylon membrane (Thermo Fisher Scientific) followed by cross-linking under conditions of ultraviolet light at 254 nm, 0.12 J cm^{-2}. The membrane was blocked in PBS with Tween (PBST) (5% nonfat milk and 0.1% Tween 20) for 1 h and subsequently incubated with anti-m^{6}A antibody (1:1000 dilution) overnight at 4°C. After washing three times in PBST buffer, the membrane was blotted with secondary antibody (anti-rabbit, 1:5000) at room temperature for 1 h. The dot blotting signal was visualized after reaction with enhanced chemiluminescence.

Flow cytometry

The cultured cells were collected by TrypLE (Thermo Fisher, Cat#12604021) and resuspended in DPBS (Dulbecco's Phosphate-Buffered Saline) supplemented with 2% FBS. After washing, the cells were incubated with diluted antibodies (APC-conjugated mouse-anti-human CD184 (BD, Cat#555976) according to the staining protocol from BD Biosciences (BD, Cat#562574). Then, the cells were washed twice and resuspended with DPBS for flow cytometry analysis on BD FACSCelesta. The data were analyzed with FlowJo software.

Statistical analyses

Information regarding error bars, numbers of replicates or samples, and statistical analyses are described in the corresponding figure legends. Representative results of at least three independent experiments are shown unless otherwise indicated.

MeRIP-seq

Total RNA from four biological replicates of each condition was poly(A)-enriched using Oligo (dT)25 and fragmented to a mean size of 200–300 nucleotides by incubation in 50 mM $MgCl_2$ for 8 min at 95°C. A portion of fragmented RNA was saved as input. The remaining RNA samples were incubated overnight at 4°C, rotating with protein G magnetic beads (NEB) coated with EpiMark anti-m^{6}A antibody (NEB). Washes and elution were performed as described above. To remove unbound RNA, samples were washed 5× with each of the following buffers: reaction buffer (150 mM NaCl, 10 mM Tris–HCl, pH 7.5, and 0.1% NP-40 in nuclease-free H_2O), low-salt reaction buffer (50 mM NaCl, 10 mM Tris–HCl, pH 7.5, and 0.1% NP-40 in nuclease-free H_2O), and high-salt reaction buffer (500 mM NaCl, 10 mM Tris–HCl, pH 7.5, and 0.1% NP-40 in nuclease-free H_2O). RNA was eluted with RLT buffer and purified with MyOne Silane Dynabeads (Thermo Fisher Scientific). RNA libraries for the RNA input, collected supernatant, and IP were constructed using a Ultra ll Directional RNA Library Prep Kit for llluminae (NEB) following the manufacturer's protocol. Sequencing was performed at GENEWIZ, INC SUZHOU (China) on an Illumina NovaSeq 6000 instrument.

MeRIP-seq data preprocessing

The human hg38 genome and list of transcripts v31 were downloaded from Gencode (https://www.gencodegenes.org/). MeRIP-seq reads were processed to eliminate adapter sequences using TrimGalore v.0.6.10 and subsequently aligned to the human reference genome with STAR 2.7.10b [40]. Reads <30 in length were removed, and only the proper pair and uniquely mapped alignments were persisted for the downstream pipelines. m^{6}A methylation peaks were identified utilizing the R package exomepeak2. High-confidence peaks were determined based on the criteria cutoff $RMP_{\_IP} > 1$, $\log_2FC > 1.5$, and the peaks score > 4. To establish a consensus peak list, we integrated peaks that were consistently detected across three samples. Only peaks present in all three replicates were retained for the final analysis. Differential methylation analysis of m^{6}A peaks was conducted using the R package limma [41]. Peaks were classified as differentially methylated based on a log fold change exceeding 1 and a significance threshold of $P < 0.05$.

hESCs cell culture and endoderm differentiation

The H9 human embryonic stem cell (hESC) line was cultured in mTeSR1 medium (STEMCELL Technologies, cat. no. AB217641) on Matrigel-coated plates (Corning, cat. no. 354277) with daily medium changes. When the cells reached 60%–70% confluence, they were washed once with DPBS (Gibco, cat. no. C14190500BT) and incubated with Accu-

tase (Sigma, cat. no. A6964-500ML) at 37°C for 3–5 min. After removing Accutase, the cells were gently resuspended in mTeSR1 medium and seeded onto Matrigel-coated six-well plates at a density of 0.5–1.0 × 10^5 cells per well.

For endoderm differentiation, H9 cells were enzymatically dissociated into single cells using Accutase and reseeded on growth factor-reduced Matrigel-coated plates (Corning, cat. no. 354230) in mTeSR1 medium. The following day, the medium was replaced with differentiation medium comprising DMEM (Gibco, cat. no. 11965092), 0.2% BSA (YEASEN, cat. no. B57370), and 1% penicillin–streptomycin (Gibco, cat. no. 15140163). On day 1, 100 ng/ml Activin A (PeproTech, cat. no. 120-14P) and 2.5 mM CHIR99021 (Selleck, cat. no. S2924) were added. For the subsequent 2 days, only 100 ng/ml Activin A was included in the medium.

Results

Red light inducible m^{6}A writing by ΔphyA/FHY1 pair

To establish m^{6}A editing system, we modified both the dCas13b protein and sgRNA component within CRISPR framework. Initially, we engineered ΔphyA to be fused with the dCas13 protein and linked FHY1 to the truncated m^{6}A methyltransferase METTL3 (METTL3 without the zinc finger RNA binding motifs, METTL3ΔZF, referred to as M3) [23], creating engineered proteins ΔphyA-dCas13b and FHY1-M3.

To evaluate the light-inducible m^{6}A writing capability of the ΔphyA/FHY1 pair, we first assessed the m^{6}A methylation potential of ΔphyA-dCas13b and FHY1-M3 upon red light stimulation. Expression of these engineered proteins in HEK293T cells was confirmed via western blot analysis (Supplementary Fig. S1). To validate red light-mediated dynamic heterodimerization, we engineered constructs by fusing a membrane-targeting peptide (CAAX) and red fluorescent protein mCherry to ΔphyA-dCas13, resulting in ΔphyA-dCas13-mCherry-CAAX, and attaching green fluorescent protein EGFP to FHY1-M3, creating FHY1-M3-EGFP. This setup facilitated the observation of the interaction under laser confocal microscopy (Supplementary Fig. S2). In the absence of red light, the green fluorescence signal of FHY1-M3-EGFP was uniformly distributed within the cell, while the red fluorescence signal of ΔphyA-dCas13b-mCherry-CAAX was predominantly localized at the cell membrane. Upon red light activation, colocalization of green and red fluorescence signals was distinctly observed, verifying the red light-induced heterodimerization of ΔphyA-dCas13 and FHY1-M3 and demonstrating the viability of this optogenetically controlled system.

Additionally, we engineered fusion proteins by linking ΔPhyA to both the C- and N-termini of dCas13b, resulting in two anchoring proteins, dCas13b-ΔPhyA and ΔPhyA-dCas13b. Subsequently, we developed two effector proteins, FHY1-M3 and FHY1-M3M14, as described in prior studies (Supplementary Fig. S3A) [23]. To verify the subcellular localization of the fusion proteins, we performed confocal microscopy, which confirmed the correct distribution of the two effector proteins and the anchor protein (Supplementary Fig. S3B).

To evaluate their efficiency in targeting specific RNA transcripts, we targeted the A1216 site within the 3′-untranslated region (UTR) of *ACTB* mRNA, which is known for its initially low m^{6}A levels [42], making it amenable to be artificial intervened. Following irradiation with or without 660 nm light (0.8 mW cm^{-2}, cyclic illumination 10 s ON and then 50 s OFF) for 24 h [36], total RNA was isolated and immunoprecipitated using anti-m^{6}A antibodies. Quantitative analysis of m^{6}A modification at the *ACTB* A1216 site was performed using RT-qPCR (MeRIP-qPCR) [43]. Our results demonstrated that the combination of ΔPhyA-dCas13b and FHY1-M3 maximally increased m^{6}A modification level upon photoexcitation, marking this pairing as the most effective for methylation activity and chosen for subsequent studies (Supplementary Fig. S4).

Enhanced m^{6}A writing by recruitment of multiple effector proteins

To further enhanced m^{6}A editing system, the ΔphyA/FHY1 pair was further tethered in the sgRNA component of CRISPR system using the widely utilized MS2–MCP system [44]. Two MS2 RNA hairpins were appended to the 3′ end of the Cas13b sgRNA enabling specific interaction with the MCP via the MS2 RNA stem-loop structure [45, 46]. MCP was then fused to ΔphyA, resulting in MCP-ΔphyA. Following red light (660 nm) exposure, FHY1-M3 is attracted not only to ΔphyA-dCas13b but also to the MS2-modified sgRNA via the MCP-ΔphyA linker. This dual recruitment strategy increases the concentration of m^{6}A methyltransferase at the target site, boosting m^{6}A writing efficiency (Fig. 1A).

To evaluate the impact of multiple effector proteins on specific RNA transcripts, we targeted the A1216 position within *ACTB* mRNA. We screened several sgRNAs with varying proximities to the A1216 site to determine the influence of sgRNA target location on editing efficiency. Among these, the MS2-tethered sgRNA positioned 22 nucleotides from the A1216 site (sgRNA-22-MS2) showed the highest m^{6}A fold changes and was therefore selected for further investigation (Fig. 1B). HEK293T cells were then transfected with plasmids encoding ΔPhyA-dCas13b, FHY1-M3 (or its catalytically inactive variant FHY1-M3*), ΔPhyA-MCP, and the modified sgRNA-22-MS2 for 24 h. Following 660 nm light irradiation for an additional 24 h, m^{6}A levels at the A1216 site of *ACTB* mRNA were measured via MeRIP-qPCR. Significant m^{6}A enrichment was observed only under red light with catalytically active METTL3 (Fig. 1C), with no increase noted for the mutated METTL3 domain (Fig. 1C). Remarkably, in the absence of ΔphyA-MCP linkage, where only ΔPhyA-dCas13b can recruit FHY1-M3 to the target site, the m^{6}A writing efficiency was considerably lower compared to samples with ΔphyA-MCP linkage (∼3-fold) (Fig. 1C). This observation underscores the effectiveness of the dual recruitment strategy in boosting m^{6}A writing efficiency. Furthermore, m^{6}A writing efficiency was found to correlate with illumination intensity, emphasizing the crucial role of light in this editing system (Supplementary Fig. S5).

Next, we utilized the SELECT method to further validate the m^{6}A modification level at the A1216 locus of *ACTB* mRNA, providing precise single-base resolution measurement of m^{6}A modifications [47]. Employing DNA oligonucleotides with PCR adapters specific to the A1216 region, we detected a reduction in full-length products under red light in our inducible m^{6}A writing system, which corroborated an increase in m^{6}A levels at the target site (Supplementary Fig. S6). Consistent with earlier MeRIP-qPCR findings (Fig. 1C),

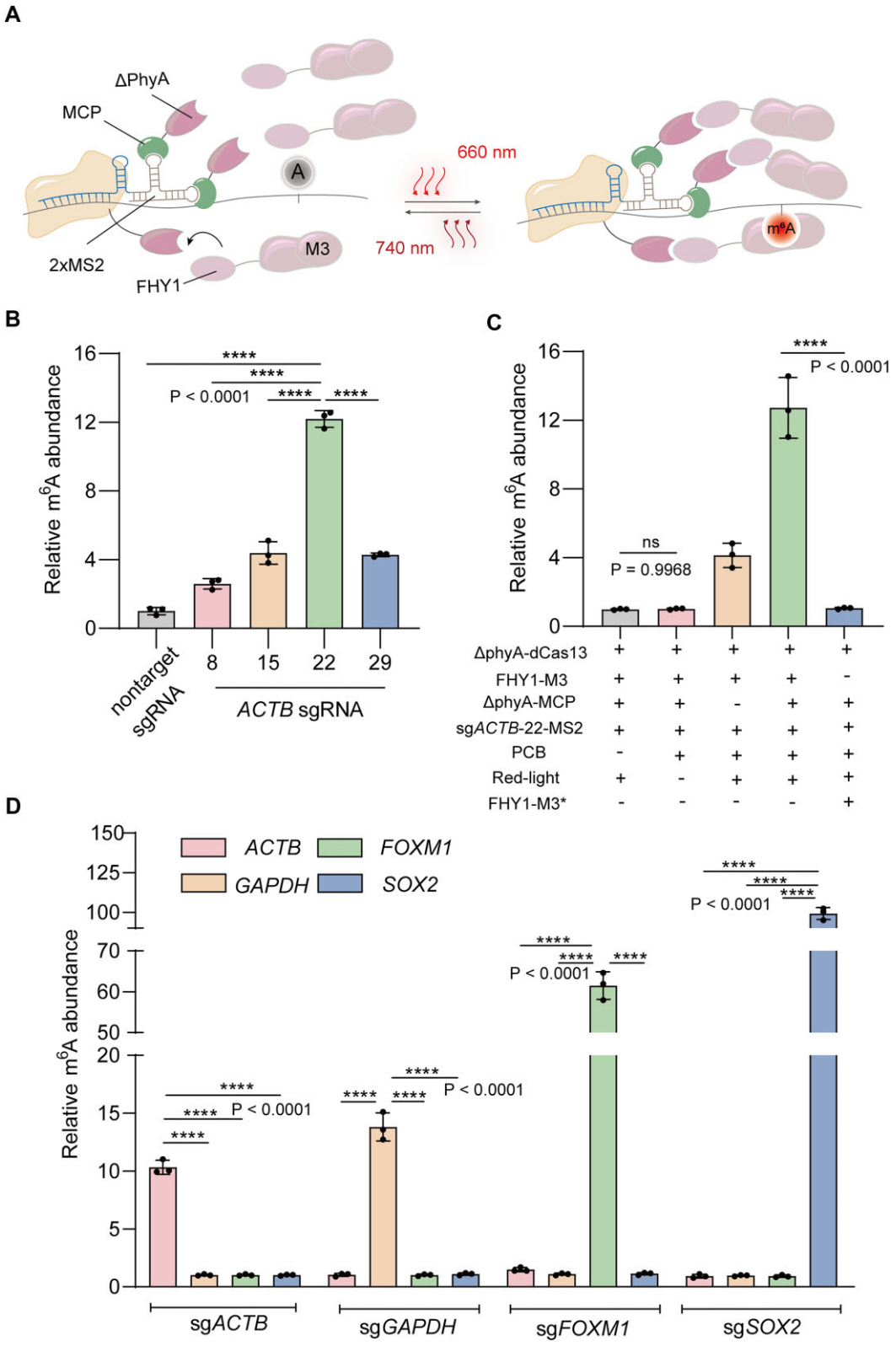

Figure 1. Red light-induced (660 nm) enhanced m^{6}A writing in HEK293T cells. (**A**) Schematic of the strategy of red light induced enhanced m^{6}A writing. (**B**) The m^{6}A level changes with different sgRNAs at the *ACTB* mRNA A1216 site. (**C**) The m^{6}A level changes under different treatment conditions at the *ACTB* mRNA A1216 site. (**D**) The relative m^{6}A level changes at different mRNA sites when using different mRNA-specific sgRNAs for editing. The concentration of the phycocyanobilin (PCB) used in the experiments is 5 μM. All results were calculated by normalization of data from each sample to that from the condition of ΔphyA-dCas13b plus sgRNA-22-MS2. Values and error bars reflect the mean, S.E.M. of three independent biological replicates. *P*-values are shown in the charts are determined by one-way ANOVA. **** represents p-value < 0.0001.

diminished m^{6}A methylation was noted in samples lacking the ΔphyA-MCP linkage, with no detectable changes observed in samples utilizing the catalytically inactive METTL3 variant (FHY1-M3*). The alignment between MeRIP-qPCR and SELECT results highlights the effectiveness of our enhanced m^{6}A editing approach, which integrates multiple effector proteins into both the dCas protein and sgRNA components.

To confirm the recruitment of FHY1-M3 to *ACTB* mRNA upon red light exposure, we conducted cross-linking immunoprecipitation followed by RT-qPCR analysis (CLIP-qPCR) [19], utilizing an anti-M3 antibody to isolate the FHY1-M3-associated target region. Upon illumination, a significant enrichment of the *ACTB* mRNA target region was observed, validating the light-induced recruitment of the METTL3 domain (Supplementary Fig. S7). Expanding beyond the *ACTB* A1216 site, we applied our m^{6}A editing system to additional RNA transcripts, including *GAPDH* A690, *FOXM1* A3488/A3504, and *SOX2* A1398/A1405 locations [23]. Following cell transfection with respective modified sgRNAs for these RNA transcripts, m^{6}A levels at these specific sites were quantified using MeRIP-qPCR. As expected, a notable increase in m^{6}A modification was detected at each targeted RNA site, demonstrating both the high efficiency of our m^{6}A editing system and its broad utility (Fig. 1D). Importantly, enhanced m^{6}A modification was exclusively observed in the targeted RNA transcript, with no detectable changes in the other three untargeted RNAs, underscoring the precise on-target efficacy of our editing approach.

The biological effects of m^{6}A writing

Prior research has shown that m^{6}A modification at the *ACTB* A1216 site reduces its mRNA stability [22]. To explore the biological consequences of targeted m^{6}A writing, we analyzed *ACTB* mRNA stability under various m^{6}A editing scenarios. Following plasmid transfection and subsequent exposure to red light (660 nm) for 24 h, RT-qPCR was conducted to assess *ACTB* mRNA abundance. The results indicated a significant reduction in *ACTB* mRNA levels upon red light activation with sgRNA-22 (Supplementary Fig. S8, green column), suggesting the increased m^{6}A modification ratio contributed to greater mRNA instability. Notably, transfection with ΔphyA-dCas13b and sgRNA-22 alone did not affect mRNA stability (Supplementary Fig. S9). We further investigated the impact of m^{6}A on the stability and translation of other RNA transcripts, specifically targeting the *FOXM1* A3488/A3504, and *SOX2* A1398/A1405, and *GAPDH* A690 sites. Introducing m^{6}A modifications at the 3′-UTR sites of *FOXM1* and *SOX2* resulted in reduced RNA stability and lower transcript levels (Fig. 2A and B), which subsequently led to decreased expression of FOXM1 and SOX2 proteins (Fig 2D and E). Consistent with previous findings, the change of RNA methylation at *GAPDH* A690 did not affect mRNA level (Fig. 2C) and corresponding protein synthesis (Fig. 2F) [22]. These findings highlight the variable regulatory roles of RNA m^{6}A modification [48, 49] and emphasize the value of the light-inducible m^{6}A editing system for probing cellular functions tied to m^{6}A dynamics.

Off-target methylation of the m^{6}A editing system in human cells

To evaluate potential off-target methylation, we first assessed the impact of the light-induced editing system on total m^{6}A content in human cells using dot-blot analysis. No significant change in m^{6}A abundance was observed compared to the control (Supplementary Fig. S10).

Then, we targeted *ACTB* A1216 with the editing system and analyzed global m^{6}A peaks via m^{6}A-seq. Consistent with MeRIP-RT-qPCR results, we observed methylation enrichment at A1216 upon cotransfection with *ACTB*-targeting guide RNA, but not with nontargeting RNA or inactive controls (Fig. 3A–C). Examination of other transcript regions revealed that only 1.8% additional m^{6}A sites were modified under the guidance of specific gRNAs, with minimal changes in off-target sites (Fig. 3D).

To confirm methylation specificity, we analyzed nearby A sites in *ACTB* mRNA using SELECT. No significant methylation changes were detected at neighboring sites compared to controls (Supplementary Fig. S11). Single-nucleotide quantification of m^{6}A at *ACTB* A1216 showed a marked increase in the experimental group (0.48 ± 0.01 fmol) relative to the nontargeting guide RNA group (0.07 ± 0.01 fmol) (Supplementary Fig. S12).

To assess the impact of off-target methylation on gene expression, we performed RNA-seq on cells transfected with the light-induced editor targeting *ACTB* A1216 and nontargeting controls or inactive controls. No significant differences in gene expression were observed, indicating minimal off-target effects on nontarget genes (Fig. 3E).

Far-red light inducible m^{6}A erasure

The enhancement of m^{6}A writing efficiency demonstrated that modifying MS2 on sgRNA can successfully recruit the effector proteins to the RNA target. Building on this approach, we next investigated the feasibility of far-red light inducible m^{6}A erasure by engineering sgRNA to incorporate the Bphp1/PspR2 pair. PspR2 was fused to the MCP protein, enabling RNA target recruitment via the formation sgRNA-MS2/MCP-PspR2 complex. Subsequently, RNA m^{6}A demethylase FTO was linked to Bhp1, resulting in Bhp1-FTO, which could be recruited by MCP-PspR2 under far-red light (740 nm) to facilitate targeted m^{6}A removal (Fig. 4A). We selected the A2577 site on the nuclear noncoding RNA *MALAT1*, known for its significant m^{6}A presence [42], as a model for this experiment. Light-induced cellular colocalization experiments confirmed the dimerization of the modified Bphp1/PspR2 pair, following separate fusion with the membrane-targeting peptide CAAX and the fluorescent proteins (Supplementary Fig. S13). To evaluate far-red light-induced m^{6}A removal at *MALAT1* A2577, all plasmids were transfected for 24 h, followed by another 24-h exposure to far-red light (740 nm, 0.2 mW cm^{-2}, cyclic illumination 15 s ON and 45 s OFF) [35]. MeRIP-qPCR results indicated m^{6}A demethylation at the *MALAT1* A2577 site occurred exclusively under the specified light condition (Fig. 4B). The SELECT method further verified these findings, showing a marked reduction in the m^{6}A ratio at the *MALAT1* m^{6}A2577 site, with no alteration at the A2511 site lacking m^{6}A modification (Supplementary Fig. S14). Additionally, other sites previously reported with higher m^{6}A levels, such as *MYC* A5553, *CYB5A* A135, and *CTNNB1* A126 [24, 25], remained unchanged when only the *MALAT1*-targeted sgRNA was utilized, highlighting the specificity of this light-inducible m^{6}A removal system (Fig. 4C). These results confirm that the light-inducible m^{6}A editing strategy can be extended to control m^{6}A erasure.

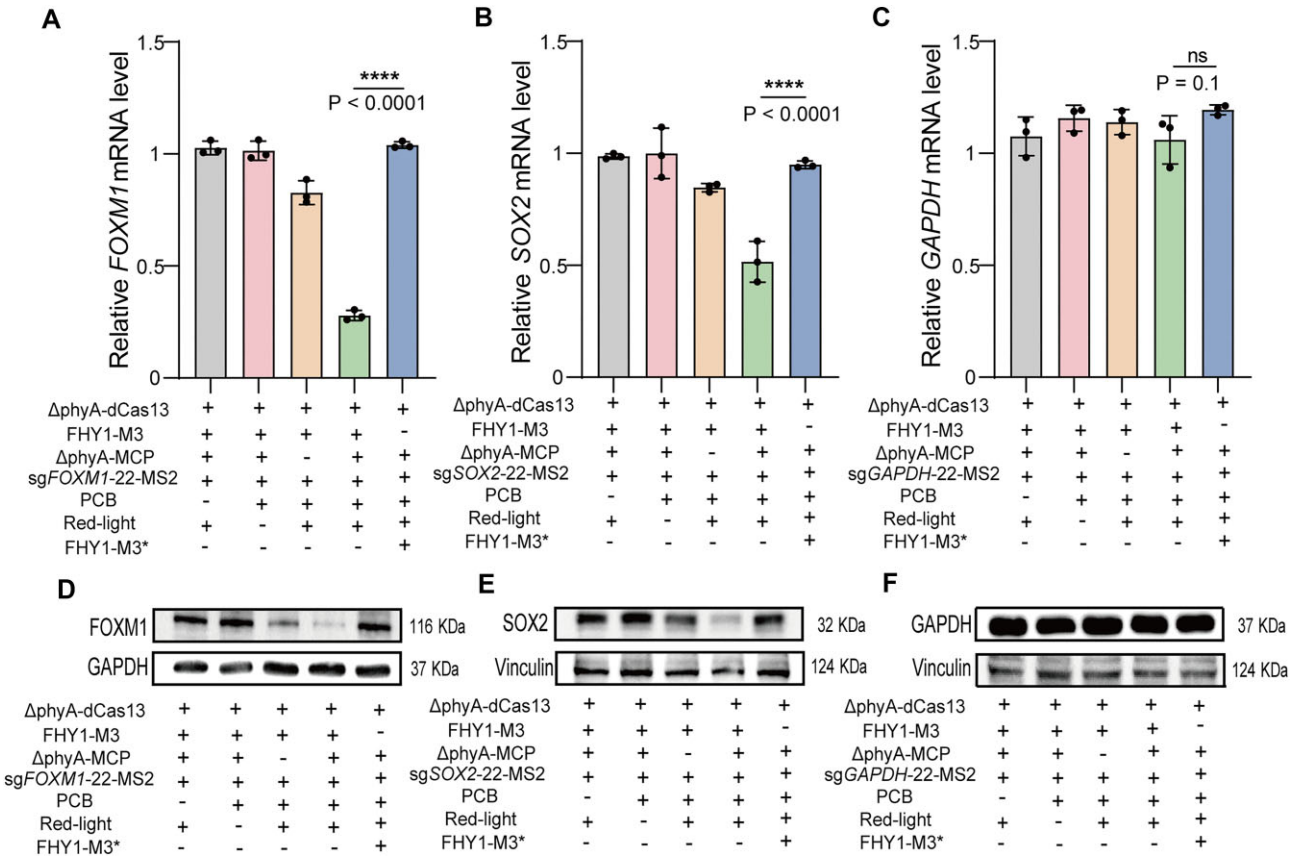

Figure 2. The biological effects of m^{6}A writing. The relative abundance of *FOXM1* (**A**), *SOX2* (**B**), *GAPDH*, and (**C**) mRNAs in HEK293 cells under different m^{6}A writing conditions. (**D–F**) Western blotting of FOXM1, SOX2, and GAPDH protein levels under different m^{6}A writing conditions. Endogenous Vinculin or GAPDH were used as the internal control. The concentration of the PCB used in the experiments is 5 μM. All results of groups in panels (A–C) with different treatments were normalized to the group of ΔphyA-dCas13b plus sgRNA-22-MS2 treatment. Values and error bars reflect the mean, S.E.M. of three independent biological replicates. *P*-values shown in the charts are determined by one-way ANOVA. **** represents p-value < 0.0001.

To further explore the influence of the proximity between sgRNA and the m^{6}A site on m^{6}A erasure efficiency, we cloned a series of sgRNAs targeting various distances from the A2577 site. Despite all sgRNAs resulting in decreased m^{6}A levels, *MALAT1* sgRNA-22 demonstrated the most efficient m^{6}A removal compared to others (Fig. 4D), mirroring the sgRNA design strategy in the m^{6}A writing system. This outcome suggests that the consistent editing sites of both m^{6}A writing and erasure can facilitate reversible m^{6}A editing within a single system, enabling dynamic controlling m^{6}A modification processes through light induction.

Photo-reversible m^{6}A editing

Traditional m^{6}A editing systems typically engage a single enzyme type, either for methylation or demethylation at a specific m^{6}A site, lacking the capability to enable concurrent m^{6}A writing and erasure [22–30]. In our system, modulated dCas13b and MS2-fused sgRNA are capable of recruiting three effector proteins, not only enhancing the modification efficiency but also offering the potential for reversible light-triggered m^{6}A editing if two synergistic pairs of heterodimeric proteins are incorporated (Fig. 5A). Specifically, plasmids encoding ΔPhyA-dCas13, FHY1-M3, MCP-PspR2, Bphp1-FTO, and sgRNA-MS2 were cotransfected into 293T cells. Red light (660 nm) activation triggers m^{6}A writing via ΔPhyA-FHY1 dimerization, while far-red light disrupts this interaction and engages PspR2-Bphp1, halting m^{6}A writing and initiating erasure. Initial investigations into the m^{6}A writing response over time revealed a swift increase in m^{6}A levels at the *ACTB* A1216 site within 4 h of red-light exposure, with a more gradual rise over a 24-h period (Supplementary Fig. S15), identifying 4 h as the optimal duration for red light-induced methylation. For the m^{6}A erasure phase, far-red light exposure (740 nm) produced a significant reduction in m^{6}A levels within 2 h (Supplementary Fig. S16), establishing this timeframe as effective for far-red light-mediated demethylation.

Subsequently, we explored reversible, light-induced m^{6}A editing at the *ACTB* A1216 and *SOX2* A1398/A1405 sites using alternating red and far-red light. After transfecting 293T cells with plasmids for 24 h, the cells underwent repeated cycles of red light (660 nm, 4 h) and far-red light (740 nm, 2 h) exposure. The m^{6}A levels, monitored over time, exhibited cyclical fluctuations with each transition between 660 and 740 nm light. (Fig. 5A and B). This dynamic pattern persisted through multiple cycles, contrasting with a steady m^{6}A level observed in the presence of nontargeting sgRNA. Additionally, without far-red light (740 nm) illumination, cycling between red light exposure (660 nm) and dark periods did not sustain reversible RNA m^{6}A editing; m^{6}A levels only increased under red light and remained constant during dark

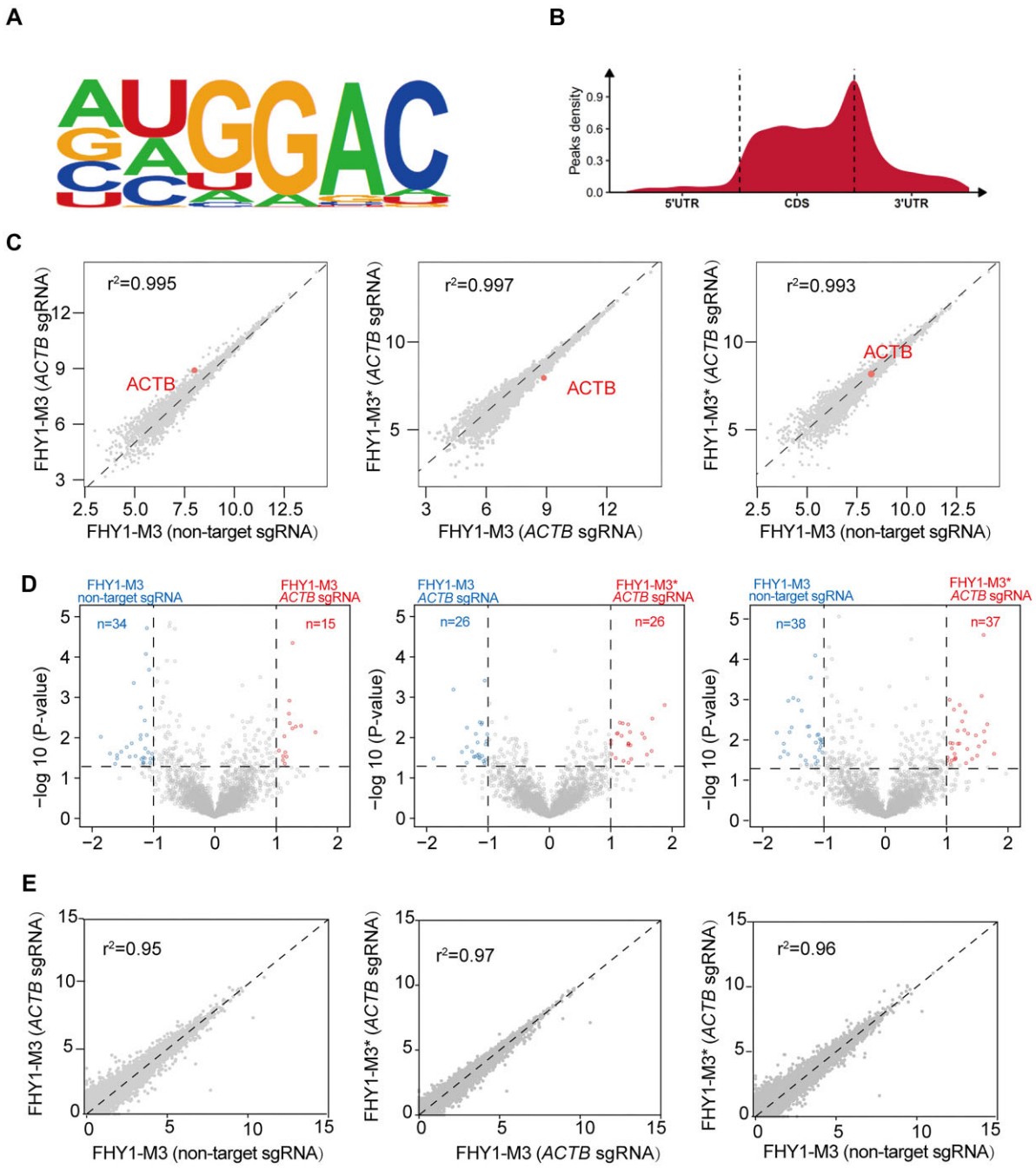

Figure 3. Specificity and off-target methylation of the light-induced editors. (**A**) Binding motif identified by HOMER with m^{6}A-seq peaks. (**B**) Distribution of m^{6}A-seq peaks across the length of mRNA. Each region of 5′-UTR, CDS, and 3′-UTR were binned into different segments according to their average legth. (**C**) Differential m^{6}A enrichment of methylated sites in HEK293T cells transduced with the light-induced editors FHY1–M3nls or FHY1–M3nls* and either *ACTB* A1216-targeting or nontargeting sgRNAs. The section represents m^{6}A methylation level changes upon the conditions quantified by m^{6}A-seq. (**D**) Differential methylation of m^{6}A sites between the conditions, indicating differentially methylated sites with statistical significance ($P < 0.05$) are shown. (**E**) Differential RNA expression of HEK293T cells transfected with the light-induced editors of FHY1–M3nls or FHY1–M3nls* and either *ACTB* A1216-targeting or nontargeting guide RNAs.

phases (Supplementary Fig. S17). To assess the impact of dynamic m^{6}A deposition/removal on mRNA levels, we measured *SOX2* and *ACTB* mRNA levels over 24 h. As m^{6}A levels fluctuated, corresponding changes in mRNA abundance were observed (Fig. 5C and D). These results validate the establishment of a photo-reversible m^{6}A editing system, employing alternating light regimes to enable precise modulation of the m^{6}A modification landscape and mRNA expression at specific genomic loci.

Dynamic m^{6}A regulation modulates hESC differentiation

Previous studies have reported that m^{6}A modifications on *SOX2* play a critical role in regulating stem cells (hESCs) differentiation [23, 50]. Inspired by this, we aimed to investigate whether our reversible m^{6}A editing system could be applied to study this process. Using the light-induced editing system described above, we assessed the functional con-

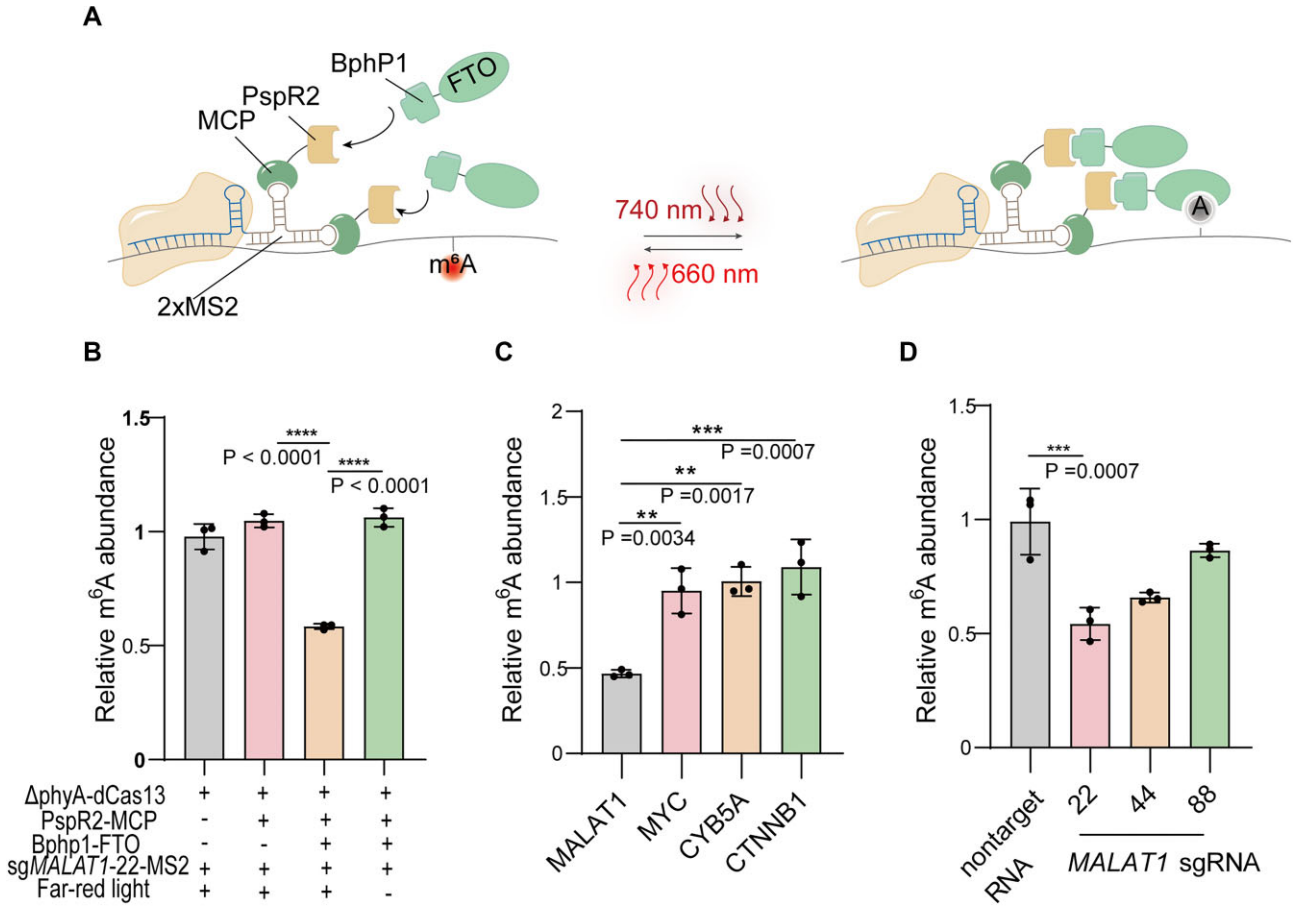

Figure 4. Far-red light induced m^{6}A erasing at the *MALAT1* RNA A2577 site in HeLa cells. (**A**) Schematic of the far-red light induced m^{6}A erasing. (**B**) The m^{6}A level changes under different editing conditions using the far-red light inducible m^{6}A erasing system. (**C**) The m^{6}A level changes at different RNA sites (*MALAT1* A2577, *MYC* A5553, *CYB5A* A135, and *CTNNB1* A126) using sgRNA targeting the *MALAT1* A2577 site. (**D**) The m^{6}A level changes using different sgRNAs. All results of groups in panels (A–C) with different treatments were normalized to the group of ΔphyA-dCas13b and sgRNA-22-MS2 treatment. Values and error bars reflect the mean, S.E.M. of three independent biological replicates. *P*-values are shown in the charts are determined by one-way ANOVA. **represents $p < 0.01$, *** represents $p < 0.001$,**** represents $p < 0.0001$.

sequences of *SOX2* A1398 demethylation on hESC differentiation [16]. Upon transfection of plasmids into hESCs, cells underwent different light exposure cycles, as previously observed, m^{6}A levels fluctuated periodically (Fig. 6A and B).

Next, we directed the endoderm differentiation of the transfected hESCs under varying light conditions. Remarkably, after differentiation induction, the editing system extended *SOX2* expression in hESCs under 740 nm light exposure, while no such effect was observed in control cells with nontargeting sgRNA (Fig. 6C). Additionally, the expression of several key endodermal genes (*SOX17*, *CXCR4*, and *FOXA2*) were obviously downregulated, while genes associated with stemness or ectodermal formation (*NANOG*, *OCT4*, and *SOX2*) were obviously upregulated (Fig. 6C), accompanied by a decrease in the proportion of endodermal cells (Fig. 6D). This effect was largely restored after exposure to 660 nm light during endoderm differentiation (Fig. 6C and D, and Supplementary Fig. S18).

These results collectively demonstrate that the dynamic regulation of a single m^{6}A site can effectively regulate the differentiation of hESCs, further emphasizing the importance of time-dependent m^{6}A-mediated post-transcriptional regulation in cell fate determination.

Discussion

Advances in CRISPR technology have enabled site-specific RNA m^{6}A editing without altering the primary sequence by fusing m^{6}A effectors to dCas proteins. Several techniques have been developed to regulate m^{6}A [22–30]. Our previous work on targeted RNA demethylation using the SunTag system [27] and sgRNA modification for live-cell RNA imaging [46]. Building on these findings, we engineered both dCas13 and sgRNA with light-inducible heterodimerizing proteins to create a reversible and enhanced m^{6}A editing system. This dual modification approach offers more versatile regulatory outcomes compared to traditional systems that modify only dCas proteins.

By incorporating the ΔphyA/FHY1 pair, our system enhances m^{6}A writing efficiency by concentrating METTL3 enzymes at the target site. Minimal off-target effects, confirmed by m^{6}A-seq and single-nucleotide quantification, ensure high specificity, enabling precise studies of m^{6}A modifications without unwanted changes in RNA levels. The addition of two heterodimer pairs, ΔphyA/FHY1 and Bphp1/PspR2, allows reciprocal activation and deactivation of m^{6}A writing and erasure, marking the first photo-reversible RNA m^{6}A editing system capable of multiple cycles. We demonstrated that dynamic m^{6}A regulation at specific mRNA sites, such as *ACTB*/*SOX2*,

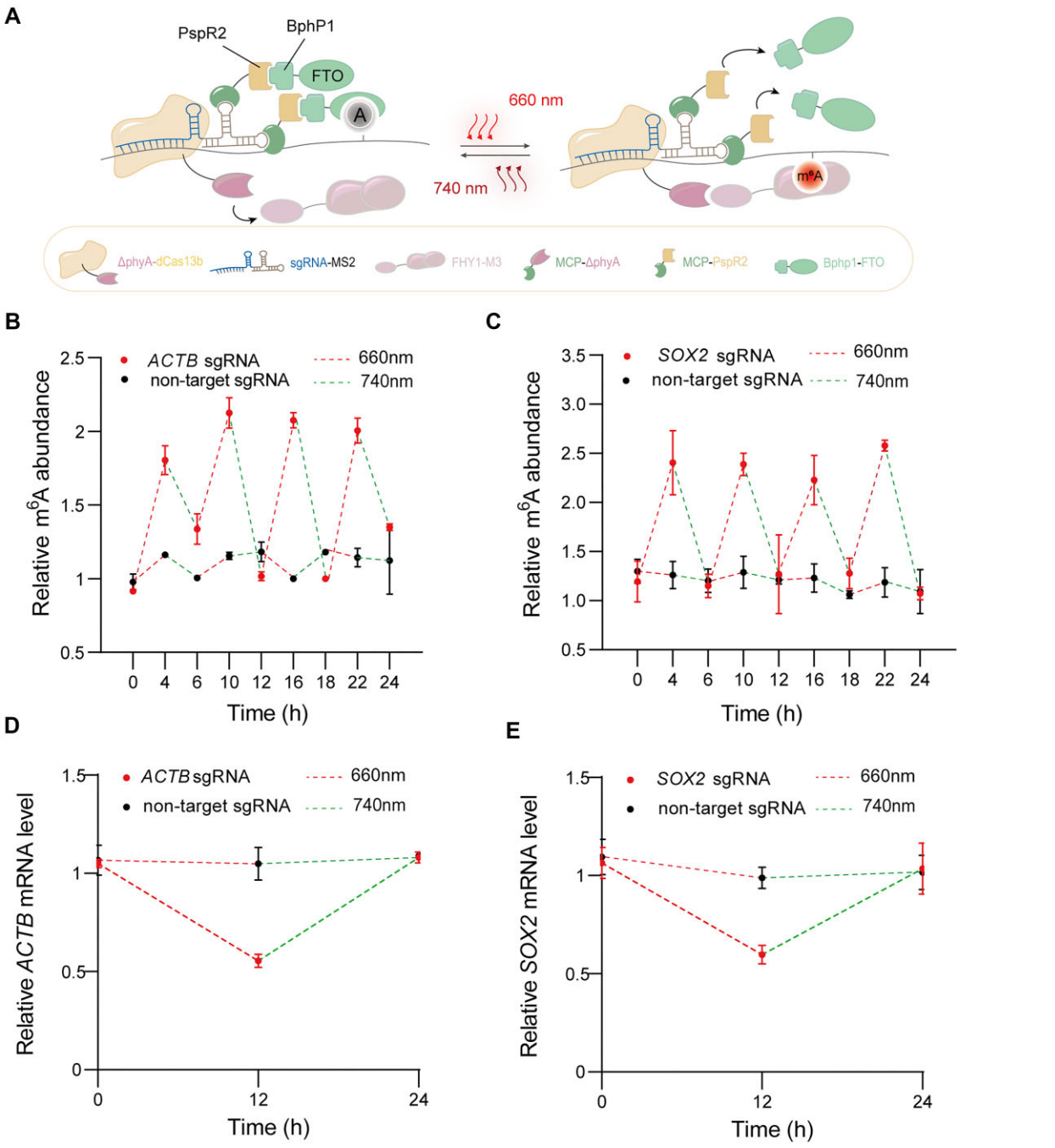

Figure 5. Photo-reversible m^{6}A editing in HEK293T cells. (**A**) Reversible RNA N6-Methyladenosine editing: ΔphyA-dCas13b and PspR2-MCP are directed to specific adenosine sites by sgRNA-MS2. Upon 660 nm red light induction, ΔphyA and FHY1 fusion proteins form a heterodimer, recruiting FHY1-M3 to the target site for m^{6}A installation. This modification can be reversed by exposure to 740 nm far-red light, which results in the release of FHY1-M3 and subsequent recruitment of Bphp1-FTO, enabling demethylation at the specific RNA site. (**B**) The relative m^{6}A levels at the *ACTB* A1216 site were reversible edited by the repeated cycles of red light (660 nm, 4 h) and far-red light (740 nm, 2 h) exposure. (**C**) The relative m^{6}A levels at the *SOX2* A1398/A1405 site were edited by the repeated cycles of red light (660 nm, 4 h) and far-red light (740 nm, 2 h) exposure. (**D** and **E**) The relative abundance of mRNA (c)*ACTB* (d)*SOX2* in 24 h. All results of groups with different treatments were normalized to the group of ΔphyA-dCas13b plus sgRNA-22-MS2 and PCB (5 μM) treatment. Values and error bars reflect the mean, S.E.M. of three independent biological replicates. *P*-values shown in the charts are determined by one-way ANOVA.

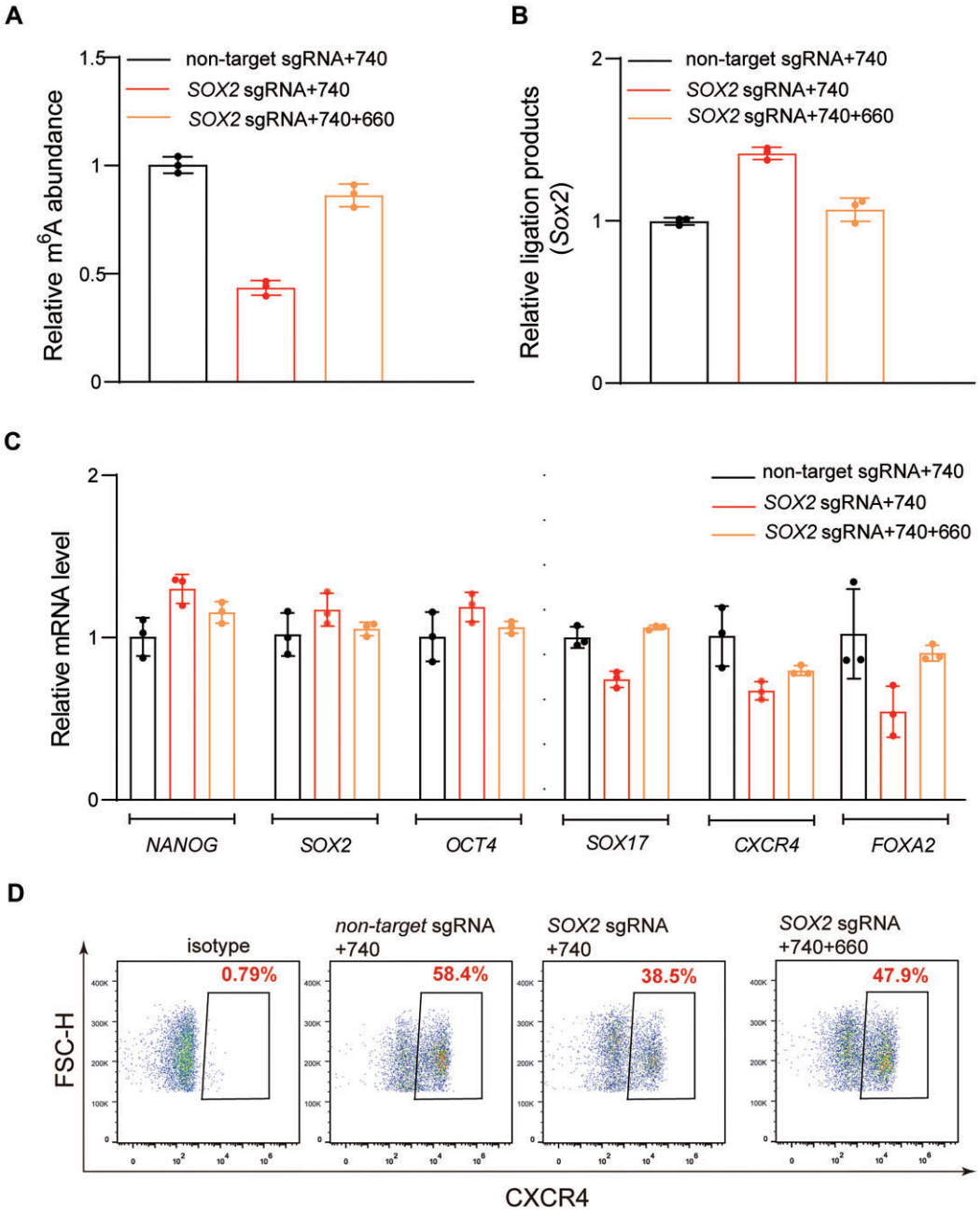

Figure 6. Dynamic m^{6}A regulation modulates hESC endoderm differentiation. (**A**) MeRIP-RT-qPCR of the relative m^{6}A levels at the *SOX2* A1398 site in hESCs transduced with the light-induced editors. The cells were reversibly edited by the far-red light (740 nm, 2 Day) or far-red/red light (740 nm, 2 Day; 660 nm,1 Day) exposure. (**B**) SELECT of the m^{6}A at the *SOX2* A1398 in hESCs upon the conditions. A lower *C*t value (i.e. a higher amount of the full-length SELECT product) indicated a lower level of m^{6}A at the probed A1398 site. (**C**) The relative mRNA abundance of *NANOG, SOX2, OCT4, SOX17, CXCR4,* and *FOXA2* in hESCs under different light exposure conditions. (**D**) Flow cytometric analysis of endoderm differentiation efficiency of hESCs by surface marker CXCR4. All results were calculated by normalizing data from each sample to that from the condition of ΔphyA-dCas13b plus sgRNA-22. Values and error bars reflect the mean, S.E.M. of three independent biological replicates. Source data are provided in the source data file.

can influence gene expression. Specifically, this system extends *SOX2* expression, inhibits endodermal differentiation in hESCs, offering a tool to control stem cell fate decisions and providing insights into the role of dynamic m^{6}A.

Our approach eliminates the need for chemical inducers like abscisic acid [28], offering a more convenient and noninvasive method for reversible RNA m^{6}A editing. The long-wavelength excitation characteristics of ΔphyA/FHY1 and Bphp1/PspR2 further enhance the system's suitability for *in vivo* applications, providing advantages over previous technologies [26]. In addition, by integrating other RNA modification effectors, this photo-inducible strategy can be expanded to various RNA modifications, thereby broadening the scope of our dynamic toolkit for precise epigenetic control.

Acknowledgements

The authors thank all members of the Zhou lab for helpful discussions and insights.

Author contributions: Heng Tang (Conceptualization, Methodology, Software, Validation, Writing—original draft, Writing—review & editing, Visualization, Funding acquisition), Shaoqing Han (Methodology, Investigation, Data curation, Writing—review & editing), Jie Yang (Investigation, Methodology, Validation, Software, Formal analysis), Xin Jiang (Investigation, Data curation), Yi Zhang (Investigation, Data curation), Junran Peng (Investigation, Data curation, Visualization), Fang Wang (Resources, Funding acquisition), Xiang Li (Conceptualization, Writing—review & editing, Resources, Funding acquisition), Xiang Zhou (Conceptualization, Writing—review & editing, Resources, Funding acquisition), Wei Jiang (Conceptualization, Supervision, Writing—review & editing), and Xiaocheng Weng (Conceptualization, Funding acquisition, Supervision, Writing—original draft, Writing—review & editing)

Supplementary data

Supplementary data is available at NAR online.

Conflict of interest

None declared.

Funding

The Ministry of Science and Technology (2023YFC3402200), the National Natural Science Foundation of China (92253202 and 22177087 to X.W.; 92153303 and 22037004 to X.Z.; 22277094 to F.W.; 22407103 to H.T.), and the Fundamental Research Funds for the Central Universities (2042023kfyq05). Funding to pay the Open Access publication charges for this article was provided by the National Natural Science Foundation of China.

Data availability

The data underlying this article are available in the article and in its online supplementary material. Sequencing data have been deposited in the NCBI Gene Expression Omnibus (GEO) under accession number (https://www.ncbi.nlm.nih.gov/geo/query/acc.cgi?acc=GSE285697).

References

1. Roundtree IA, Evans ME, Pan T *et al.* Dynamic RNA modifications in gene expression regulation. *Cell* 2017;**169**:1187–200. https://doi.org/10.1016/j.cell.2017.05.045
2. Meyer KD, Jaffrey SR. The dynamic epitranscriptome: n6-methyladenosine and gene expression control. *Nat Rev Mol Cell Biol* 2014;**15**:313–26. https://doi.org/10.1038/nrm3785
3. Liu J, Yue Y, Han D *et al.* A METTL3–METTL14 complex mediates mammalian nuclear RNA N6-adenosine methylation. *Nat Chem Biol* 2014;**10**:93–5. https://doi.org/10.1038/nchembio.1432
4. Ping X-L, Sun B-F, Wang L *et al.* Mammalian WTAP is a regulatory subunit of the RNA N6-methyladenosine methyltransferase. *Cell Res* 2014;**24**:177–89. https://doi.org/10.1038/cr.2014.3
5. Schwartz S, Mumbach MR, Jovanovic M *et al.* Perturbation of m^{6}A writers reveals two distinct classes of mRNA methylation at internal and 5′ sites. *Cell Rep* 2014;**8**:284–96. https://doi.org/10.1016/j.celrep.2014.05.048
6. Jia G, Fu Y, Zhao X *et al.* N6-Methyladenosine in nuclear RNA is a major substrate of the obesity-associated FTO. *Nat Chem Biol* 2011;**7**:885–7. https://doi.org/10.1038/nchembio.687
7. Zheng G, Dahl JA, Niu Y *et al.* ALKBH5 is a mammalian RNA demethylase that impacts RNA metabolism and mouse fertility. *Mol Cell* 2013;**49**:18–29. https://doi.org/10.1016/j.molcel.2012.10.015
8. Wang X, Lu Z, Gomez A *et al.* N6-methyladenosine-dependent regulation of messenger RNA stability. *Nature* 2014;**505**:117–20. https://doi.org/10.1038/nature12730
9. Huang H, Weng H, Sun W *et al.* Recognition of RNA N6-methyladenosine by IGF2BP proteins enhances mRNA stability and translation. *Nat Cell Biol* 2018;**20**:285–95. https://doi.org/10.1038/s41556-018-0045-z
10. Yang Y, Hsu PJ, Chen Y-S *et al.* Dynamic transcriptomic m^{6}A decoration: writers, erasers, readers and functions in RNA metabolism. *Cell Res* 2018;**28**:616–24. https://doi.org/10.1038/s41422-018-0040-8
11. Meyer KD, Patil DP, Zhou J *et al.* 5′ UTR m^{6}A promotes cap-independent translation. *Cell* 2015;**163**:999–1010. https://doi.org/10.1016/j.cell.2015.10.012
12. Xiao W, Adhikari S, Dahal U *et al.* Nuclear m^{6}A reader YTHDC1 regulates mRNA splicing. *Mol Cell* 2016;**61**:507–19. https://doi.org/10.1016/j.molcel.2016.01.012
13. Zhou KI, Shi H, Lyu R *et al.* Regulation of co-transcriptional pre-mRNA splicing by m^{6}A through the low-complexity protein hnRNPG. *Mol Cell* 2019;**76**:70–81. https://doi.org/10.1016/j.molcel.2019.07.005
14. Haussmann IU, Bodi Z, Sanchez-Moran E *et al.* m^{6}A potentiates Sxl alternative pre-mRNA splicing for robust Drosophila sex determination. *Nature* 2016;**540**:301–4. https://doi.org/10.1038/nature20577
15. Wen S, Wei Y, Zen C *et al.* Long non-coding RNA NEAT1 promotes bone metastasis of prostate cancer through N6-methyladenosine. *Mol Cancer* 2020;**19**:171. https://doi.org/10.1186/s12943-020-01293-4
16. Chen X, Zhao Q, Zhao YL *et al.* Targeted RNA N6-methyladenosine demethylation controls cell fate transition in human pluripotent stem cells. *Adv Sci* 2021;**8**:2003902. https://doi.org/10.1002/advs.202003902
17. Cheng W, Liu F, Ren Z *et al.* Parallel functional assessment of m^{6}A sites in human endodermal differentiation with base editor screens. *Nat Commun* 2022;**13**:478. https://doi.org/10.1038/s41467-022-28106-0
18. Jinek M, Chylinski K, Fonfara I *et al.* A programmable dual-RNA-guided DNA endonuclease in adaptive bacterial immunity. *Science* 2012;**337**:816–21. https://doi.org/10.1126/science.1225829
19. Abudayyeh OO, Gootenberg JS, Essletzbichler P *et al.* RNA targeting with CRISPR–Cas13. *Nature* 2017;**550**:280–4. https://doi.org/10.1038/nature24049
20. Konermann S, Lotfy P, Brideau NJ *et al.* Transcriptome engineering with RNA-targeting type VI-D CRISPR effectors. *Cell* 2018;**173**:665–76. https://doi.org/10.1016/j.cell.2018.02.033
21. Anzalone AV, Koblan LW, Liu DR. Genome editing with CRISPR–Cas nucleases, base editors, transposases and prime editors. *Nat Biotechnol* 2020;**38**:824–44. https://doi.org/10.1038/s41587-020-0561-9
22. Liu X-M, Zhou J, Mao Y *et al.* Programmable RNA N6-methyladenosine editing by CRISPR–Cas9 conjugates. *Nat Chem Biol* 2019;**15**:865–71. https://doi.org/10.1038/s41589-019-0327-1
23. Wilson C, Chen PJ, Miao Z *et al.* Programmable m^{6}A modification of cellular RNAs with a Cas13-directed methyltransferase. *Nat Biotechnol* 2020;**38**:1431–40. https://doi.org/10.1038/s41587-020-0572-6
24. Wang H, Chiang C-M, Luo N *et al.* Targeted mRNA demethylation using an engineered dCas13b–ALKBH5 fusion protein. *Nucleic Acids Res* 2020;**48**:5684–94.

25. Xia Z, Tang M, Ma J *et al.* Epitranscriptomic editing of the RNA N6-methyladenosine modification by dCasRx conjugated methyltransferase and demethylase. *Nucleic Acids Res* 2021;**49**:7361–74. https://doi.org/10.1093/nar/gkab517
26. Zhao J, Li B, Ma J *et al.* Photoactivatable RNA N6-methyladenosine editing with CRISPR–Cas13. *Small* 2020;**16**:e1907301. https://doi.org/10.1002/smll.201907301
27. Mo J, Chen Z, Qin S *et al.* TRADES: targeted RNA demethylation by SunTag system. *Adv Sci* 2020;**7**:2001402. https://doi.org/10.1002/advs.202001402
28. Shi H, Xu Y, Tian N *et al.* Inducible and reversible RNA N6-methyladenosine editing. *Nat Commun* 2022;**13**:1958. https://doi.org/10.1038/s41467-022-29665-y
29. Xu Y, Wang Y, Liang FS . Site-specific m^{6}A erasing via conditionally stabilized CRISPR–Cas13b editor. *Angew Chem Int Ed* 2023;**62**:e202309291. https://doi.org/10.1002/anie.202309291
30. Xu Y, Tian N, Shi H *et al.* A split CRISPR/Cas13b system for conditional RNA regulation and editing. *J Am Chem Soc* 2023;**145**:5561–9. https://doi.org/10.1021/jacs.3c01087
31. Sharrock RA, Quail PH . Novel phytochrome sequences in Arabidopsis thaliana: structure, evolution, and differential expression of a plant regulatory photoreceptor family. *Genes Dev* 1989;**3**:1745–57. https://doi.org/10.1101/gad.3.11.1745
32. Kami CMK, Muramoto T, Yokota A *et al.* Complementation of phytochrome chromophore-deficient Arabidopsis by expression of phycocyanobilin:ferredoxin oxidoreductase. *Proc Natl Acad Sci USA* 2004;**101**:1099–104. https://doi.org/10.1073/pnas.0307615100
33. Kojadinovic M, Laugraud A, Vuillet L *et al.* Dual role for a bacteriophytochrome in the bioenergetic control of Rhodopsdeudomonas palustris: enhancement of photosystem synthesis and limitation of respiration. *Biochim Biophys Acta* 2008;**1777**:163–72. https://doi.org/10.1016/j.bbabio.2007.09.003
34. Bellini D, Papiz MZ . Structure of a bacteriophytochrome and light-stimulated protomer swapping with a gene repressor. *Structure* 2012;**20**:1436–46. https://doi.org/10.1016/j.str.2012.06.002
35. Kaberniuk AA, Shemetov AA, Verkhusha VV . A bacterial phytochrome-based optogenetic system controllable with near-infrared light. *Nat Methods* 2016;**13**:591–7. https://doi.org/10.1038/nmeth.3864
36. Zhou Y, Kong D, Wang X *et al.* A small and highly sensitive red/far-red optogenetic switch for applications in mammals. *Nat Biotechnol* 2022;**40**:262–72. https://doi.org/10.1038/s41587-021-01036-w
37. Nihongaki Y, Kawano F, Nakajima T *et al.* Photoactivatable CRISPR–Cas9 for optogenetic genome editing. *Nat Biotechnol* 2015;**33**:755–60. https://doi.org/10.1038/nbt.3245
38. He L, Zhang Y, Ma G *et al.* Near-infrared photoactivatable control of Ca^{2+} signaling and optogenetic immunomodulation. *eLife* 2015;**4**:e10024. https://doi.org/10.7554/eLife.10024
39. Wang Z, Hu M, Ai X *et al.* Near-infrared manipulation of membrane ion channels via upconversion optogenetics. *Adv Biosys* 2019;**3**:1800233. https://doi.org/10.1002/adbi.201800233
40. Dobin A, Davis CA, Schlesinger F *et al.* STAR: ultrafast universal RNA-seq aligner. *Bioinformatics* 2013;**29**:15–21. https://doi.org/10.1093/bioinformatics/bts635
41. Ritchie ME, Phipson B, Wu D *et al.* limma powers differential expression analyses for RNA-sequencing and microarray studies. *Nucleic Acids Res* 2015;**43**:e47. https://doi.org/10.1093/nar/gkv007
42. Liu N, Parisien M, Dai Q *et al.* Probing N6-methyladenosine RNA modification status at single nucleotide resolution in mRNA and long noncoding RNA. *RNA* 2013;**19**:1848–56. https://doi.org/10.1261/rna.041178.113
43. Dominissini D, Moshitch-Moshkovitz S, Salmon-Divon M *et al.* Transcriptome-wide mapping of N6-methyladenosine by m^{6}A-seq based on immunocapturing and massively parallel sequencing. *Nat Protoc* 2013;**8**:176–89. https://doi.org/10.1038/nprot.2012.148
44. Johansson HE, Dertinger D, LeCuyer KA *et al.* A thermodynamic analysis of the sequence-specific binding of RNA by bacteriophage MS2 coat protein. *Proc Natl Acad Sci USA* 1998;**95**:9244–9https://doi.org/10.1073/pnas.95.16.9244
45. Zalatan JG, Lee ME, Almeida R *et al.* Engineering complex synthetic transcriptional programs with CRISPR RNA scaffolds. *Cell* 2015;**160**:339–50. https://doi.org/10.1016/j.cell.2014.11.052
46. Tang H, Peng J, Peng S *et al.* Live-cell RNA imaging using the CRISPR–dCas13 system with modified sgRNAs appended with fluorescent RNA aptamers. *Chem Sci* 2022;**13**:14032–40. https://doi.org/10.1039/D2SC04656C
47. Xiao Y, Wang Y, Tang Q *et al.* An elongation- and ligation-based qPCR amplification method for the radiolabeling-free detection of locus-specific N(6)-methyladenosine modification. *Angew Chem Int Ed* 2018;**57**:15995–6000. https://doi.org/10.1002/anie.201807942
48. Choi J, Ieong K-W, Demirci H *et al.* N6-methyladenosine in mRNA disrupts tRNA selection and translation-elongation dynamics. *Nat Struct Mol Biol* 2016;**23**:110–5. https://doi.org/10.1038/nsmb.3148
49. Agalarov SC, Sakharov PA, Fattakhova DK *et al.* Internal translation initiation and eIF4F/ATP-independent scanning of mRNA by eukaryotic ribosomal particles. *Sci Rep* 2014;**4**:4438. https://doi.org/10.1038/srep04438
50. Molinie B, Wang J, Lim KS *et al.* m(6)A-LAIC-seq reveals the census and complexity of the m (6)A epitranscriptome. *Nat Methods* 2016;**13**:692–8. https://doi.org/10.1038/nmeth.3898

Received: June 3, 2024. **Revised:** January 3, 2025. **Editorial Decision:** February 19, 2025. **Accepted:** February 25, 2025